Internal damping measurements of additively manufactured stainless steel beams FREE

Peter K. Jensen; Joshua T. Mills; Micah R. Shepherd

Check for updates

View Online   Export Citation

Articles You May Be Interested In

Sound preservation at the Grand Mosque of Yogyakarta in Indonesia: The acoustic performance of the traditional architecture

AIP Conference Proceedings (June 2018)

Mixed method in acoustic comfort measurement to reveal component of acoustics preservation

AIP Conf. Proc. (June 2019)

Viscous-to-viscoelastic transition in phononic crystal and metamaterial band structures

J. Acoust. Soc. Am. (November 2015)

Internal damping measurements of additively manufactured stainless steel beams

Peter K. Jensen, Joshua T. Mills and Micah R. Shepherd
Department of Physics and Astronomy, Brigham Young University, Provo, UT, 84602; peterkj@byu.edu; jmills27@byu.edu; micah_shepherd@byu.edu

Modern additive manufacturing techniques have enabled an endless number of design possibilities. Naturally, it is important to understand how material properties, including the internal damping, differ for these structures. An experimental procedure has been developed to measure the internal damping of metal beams in the audial range by minimizing the effects of energy dissipation through the supports and acoustic radiation into the surrounding air. Loss factor measurements for steel and stainless steel beams manufactured traditionally are compared to samples constructed by powder bed fusion at varying angles. The results are also compared to Zener's thermoelasticity model, developed for isotropic Euler beams in flexure. Differences in the internal damping due to the manufacturing technique are identified and their deviation from Zener's theory is explored.

1. INTRODUCTION

Additive manufacturing (AM) techniques enable the fabrication of complex solid metal parts and as manufacturers seek both higher quality and efficiency, it is important to understand how these procedures affect the resulting materials' response to vibration. This can be quantified by measuring the internal damping, which describes how a material dissipates vibrational energy irrespective of exterior effects. This is a difficult value to isolate—in metals, the internal damping is typically very small—but an accurate measurement is important for proper frequency response modeling, especially when small dimensions mean that the internal damping is a dominant damping mechanism.

In this work, Euler beams were manufactured using additive powder bed fusion and their internal damping was measured. The first section of this paper reviews thin beam vibration with free boundary conditions (Sec. 1.A). We then introduce theory for internal damping in metals (Sec. 1.B). Next, Sec. 2 describes the procedure we use to measure internal damping, followed by details on the preparation of the AM specimens investigated (Sec. 3). Finally, we present our results in Sec. 4 and our conclusions in Sec. 5.

A. FLEXURAL BEAM VIBRATION

The internal damping of a metal can be measured using the simplified geometry of a rectangular beam. When the width is small and the thickness is very small compared to its length, a beam can be described by Euler-Bernoulli beam theory. The beam's composition is assumed to be isotropic, homogeneous, and linearly-elastic. This allows for the approximation that all deflection occurs in a single spatial dimension: longitudinal and torsional effects are not considered.

The deflection, y, of a thin beam satisfies the partial differential equation,

$$EI\,\frac{\partial^4 y}{\partial x^4} = -\rho A\,\frac{\partial^2 y}{\partial t^2},\tag{1}$$

where E is the Young modulus and I represents the second moment of the beam cross section. ρ gives the material density and A is the beam cross sectional area. For a beam with a rectangular cross section, I and A are functions of the width (w) and height (h, parallel to deflection), $A = wh$ and $I = wh^3/12$.

Free boundary conditions are satisfied when the moment and shear force, which are proportional to the second and third spatial derivatives of deflection respectively, are zero at the boundaries. Under these conditions, Eq. (1) yields the spatial solution,

$$y(x) = \big(\sin(kx) + \sinh(kx)\big) + \big(\cos(kx) + \cosh(kx)\big)\left(\frac{\sin(kL) - \sinh(kL)}{-\cos(kL) + \cosh(kL)}\right),\tag{2}$$
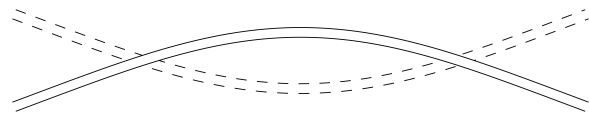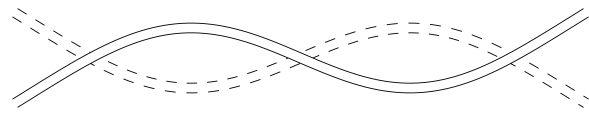
where L is the length of the beam and k is the flexural wavenumber. Mode shapes (see Table 1) are found by solving the transcendental equation, Eq. (3), for $k_n L$ and inserting each value into Eq. (2) to determine $y_n(x)$. We use these mode shapes to find the nodal locations at which the beam is supported as described in Sec. 2. $k_n L$ is also used to find the respective natural frequencies of the beam, shown in Eq. (4).

$$\cos(kL)\cosh(kL) = 1\tag{3}$$

$$f_n = \frac{1}{2\pi}\left(\frac{k_n L}{L}\right)^2\sqrt{\frac{EI}{\rho A}}\tag{4}$$

Experimental measurements of a beam's modal frequencies can be used to determine the Young modulus from Eq. (4). This is the method by which we obtain the values reported in Table 2.

Table 1: First four mode shapes of a free-free Euler beam and the corresponding value for $k_n L$.

n	Mode shape	$k_n L$
1		4.7300
2		7.8532
3		10.996
4		14.137

B.   INTERNAL DAMPING

Thermoelastic currents are generally thought to be a metal structure's primary internal damping mechanism in the audial range (Pierce, 2010, pp. 4–5). Zener's theory of thermoelasticity (Zener, 1937, 1938) describes the thermal conduction of a beam vibrating at its flexural modes. Zener models the loss factor of a material with a frequency-dependent relaxation peak, given in Eq. (5). Classically, Zener's model is denoted in terms of the relaxation time, τ, defined in Eq. (6).

$$\eta = \frac{E\alpha^2 T}{\rho\, C_s}\left(\frac{\omega\tau}{1+(\omega\tau)^2}\right) \tag{5}$$

$$\tau = \frac{h^2 \rho\, C_s}{\pi^2 \kappa} \tag{6}$$

Here, η is the damping loss factor, h is again the height of the beam, and T is the temperature which is treated as constant. As Zener's model describes thermal currents, it also includes several thermodynamic constants including the thermal expansion coefficient, α; the thermal conductivity, κ; and the specific heat capacity per unit mass, C_s. Care should be taken as some representations of this model instead use the volumetric heat capacity, $C_V = \rho C_s$. At resonance, the loss factor is the inverse of the quality factor, $Q = \eta^{-1}$, and double the damping ratio, $\zeta = \eta/2$. In this paper, we solely report internal damping using the loss factor.

An improvement to Zener's model was developed by Lifshitz and Roukes (2000), given in Eq. (7), which is expressed in terms of the normalized frequency, ξ, defined in Eq. (8). This model is further discussed by Zacharias *et al.* (2022) and Yang *et al.* (2021).

$$\eta = \frac{E\alpha^2 T}{\rho\, C_s}\left(\frac{6}{\xi^2} - \frac{6}{\xi^3}\frac{\sin\xi + \sinh\xi}{\cos\xi + \cosh\xi}\right) \tag{7}$$

$$\xi = h\sqrt{\frac{\omega\rho\, C_s}{2\kappa}} \tag{8}$$

We measure damping experimentally at each natural frequency of the beam by using the half-power method, a technique acknowledged by Zener (1938, pp. 92). Among a variety of methods, this one is both simple and accurate when damping is small ($\eta < 0.1$; Casiano, 2016, Sec. 1.1). This measurement of the loss factor is found by dividing the width of the resonance curve at the point of half power, $f_u - f_l$, by the peak frequency, f_n.

$$\eta_n \approx \frac{f_u - f_l}{f_n} \qquad (9)$$

2. METHODS

The precise measurement of internal damping requires its isolation from other damping mechanisms, primarily energy dissipation through boundary conditions and acoustic radiation into a surrounding medium. We achieve these conditions by supporting the beam on thin nylon strings and placing it inside a vacuum chamber maintained at a gauge pressure of approximately 0.5 Torr. The beam is excited remotely by an automated force hammer and its deflection is measured as a velocity through the chamber's glass dome via laser vibrometry (see Fig. 1). Both the excitation and measurement locations are near the center of the beam, but not on any nodal lines.
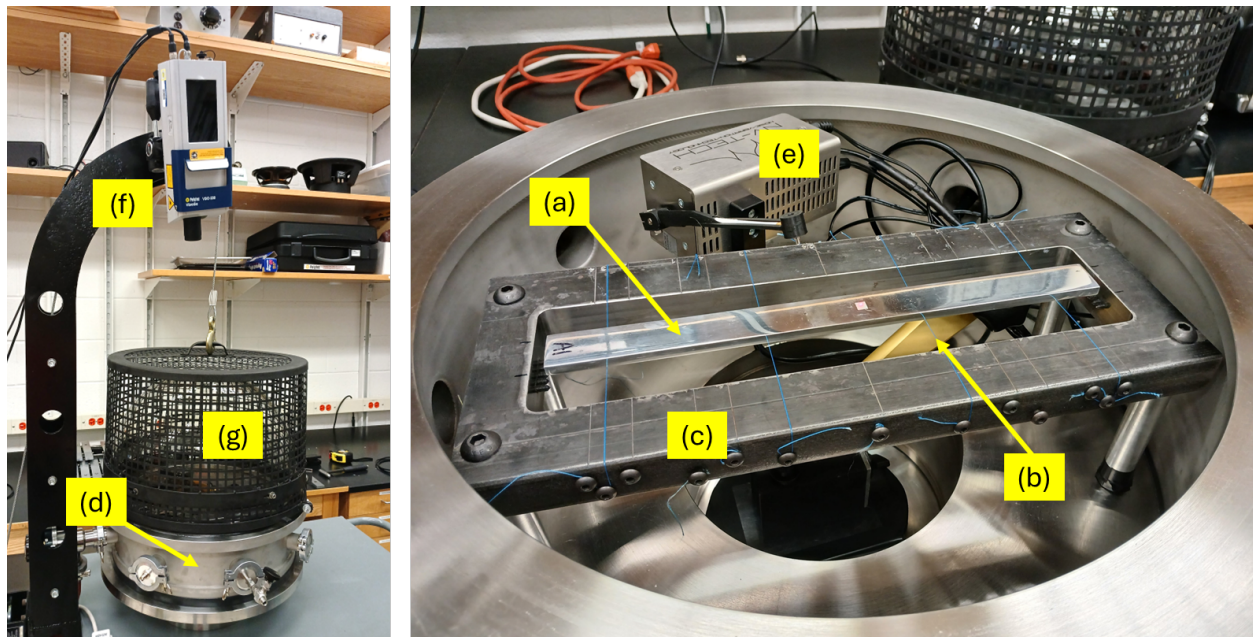
Figure 1: Experimental setup. The Euler beam (a) is supported at nodal locations by fishing line (b) strung on a support frame (c). Inside the vacuum chamber (d), an automatic force hammer (e) excites the beam which is measured using a laser Doppler vibrometer (f) through the glass dome of the vacuum chamber (g).

Once a vacuum is pulled, the beam is excited and its velocity is recorded for 30 seconds. The signal is then transformed into a power spectral density. A loss factor is calculated for each modal peak using the half-power method mentioned above (Sec. 1.B) and averaged between five identical tests. Upon excitation, the beam's motion is in a superposition of its natural modes. Normally, energy dissipation through the supporting strings is inevitable. However, by placing the support strings at the exact nodal locations of a specific spatial mode, any damping caused by the string at that particular frequency is eliminated. This means that with perfect placement, neither string tension nor beam weight will affect the measurement. By

repeating measurements with various string configurations corresponding to different modes of interest, the frequency-dependent behavior of internal damping in a particular material can be determined. We conducted measurements with the strings configured for each of the first four beam modes. As expected, the loss factor for a particular mode was lowest when measured with its corresponding string configuration. For higher modes, the minimum value from the four tests was used. For more detail about the string's effect on the loss factor, see Appendix A.

3.   SPECIMENS

This experimental setup has been used to measure the loss factors for several traditional metals including aluminum, bronze, cast iron, steel, and stainless steel (Mills *et al.*, 2024) using beams of 30 cm in length, 2.5 cm in width, and 6 mm in height. Our goal was to use AM technology to build metal beams of the same dimensions and compare their internal damping to these traditional counterparts. Four beams were constructed from 316L stainless steel by selective laser melting (SLM), a powder bed fusion method for additive metal printing. The prints were provided by the Additive Manufacturing Lab of Brigham Young University's (BYU) College of Engineering. The AM beams were constructed using the Concept Laser M2 cusing Multilaser machine. SLM involves high power lasers which melt metal powder into a solid structure. The twin lasers in this particular machine were run with a power of 400 W, a scanning speed of 2600 mm s^{-1}, and a spot size of 45 μm. The material properties of the AM and traditional samples are shown in Table 2.

Two beams were constructed perpendicular to the build plate, straight upwards at a 90° angle, and two were built at a 60° angle in order to give some insight into the effect of the SLM layer anisotropy on internal damping. The beams were built at steep angles due to limitations of the machine's build plate. Unfortunately, building specimens to this height introduced several complications including the need for a large volume of powder and subsequent interruptions in the build process. This caused a clear discontinuity about halfway through the beams and another near the end of the 90° beams. Interruptions would have been accompanied by the quenching and reheating of the beams, inciting further uncertainty in their overall uniformity. Features of concern are labeled in Fig. 2.
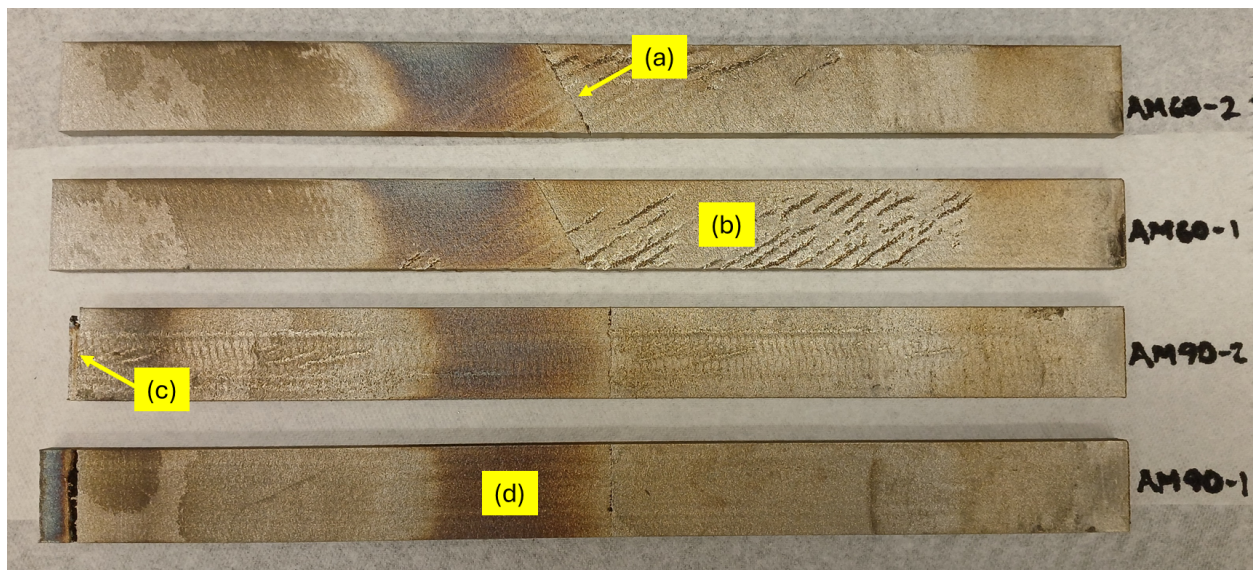
Figure 2: AM beams before being sanded and polished. A discontinuity exists where the build was restarted, indicated by (a). Surface-level porosity (b), incompletion of one of the beams (c), and discoloration indicating possible effects from heating (d) are also evident. The build direction is from right to left.

All four beams were measured in both their raw and sanded states. Additionally, one of each angle of beam was cut into smaller 13 cm pieces (see Fig. 3). A shorter beam length means there are fewer modes to measure since many of the natural frequencies are scaled above the hammer's response. However, using shorter beams removed the adverse effects of the central discontinuities and incomplete beams. This also allowed for the comparison between material at different elevations of the SLM build from before and after the first interruption occurred.
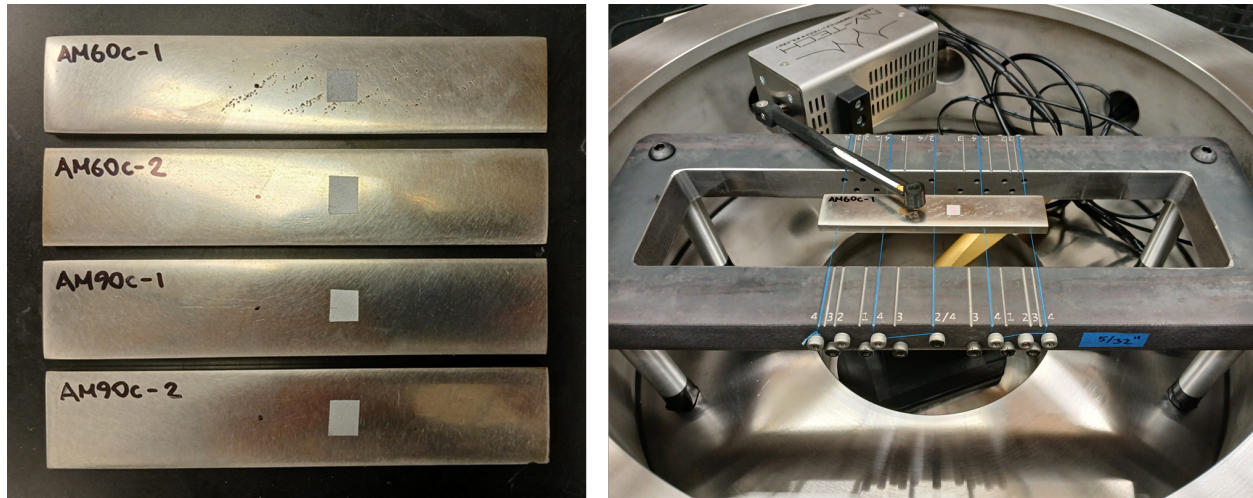

Figure 3: (left) The four resulting 13 cm beams cut and sanded from AM90-1 and AM60-1 as labeled in Fig. 2. The build direction is again from right to left. (right) The experimental setup adapted for the shorter-length beams.

4. RESULTS

Using the experimental procedure described in Sec. 2, the loss factors for each of the four AM beams were measured (see Fig. 4). Then, each beam was sanded and polished, and measurements were repeated. Sanding the AM beams had a very small effect on their measured damping (compare the dotted and solid lines in Fig. 4). A much more prominent feature the data reveals is an abrupt increase in damping at the odd ($n = 1, 3, 5$, etc.) modes compared to the damping values of the even ($n = 2, 4, 6$, etc.) modes. This behavior is not characteristic of Zener's model and is most prominent in the 90° beams. Instead, it can be explained by considering the central discontinuity in each beam. Common among the even mode shapes is a nodal line at the center of the beam (see Table 1), so there is very little deflection at the discontinuity in these frequencies. Contrarily, odd mode shapes have greater motion where the discontinuity lies. This imparts additional damping in this region due to increased asperity contact. This means that the discontinuity creates additional friction which damps the beam's motion primarily in the odd modes while the even modes are relatively unaffected. The 90° beams display a stronger effect because their discontinuities line up better with the central nodal lines whereas the 60° beam discontinuities are slanted and less central (see Fig. 2), therefore affecting the various modes more impartially.

As previously mentioned, two beams were cut into smaller 13 cm beams. Figure 5 shows the measured loss factors of these beams against those of their parent beams, shown in blue in Figs. 4 and 5. Although fewer modes are measured, the material discontinuity has been removed, yielding a flatter response in the loss factor. Two interesting features can be noted in this data. First, the 90° beams have consistently higher loss factors that the 60° beams. Second, for both the 60° and 90° beams, the beam that came from the lower part of its parent beam (i.e., the portion built first, shown in red) has a higher loss factor than the upper portion (shown in yellow). It appears that the material does indeed change with height.
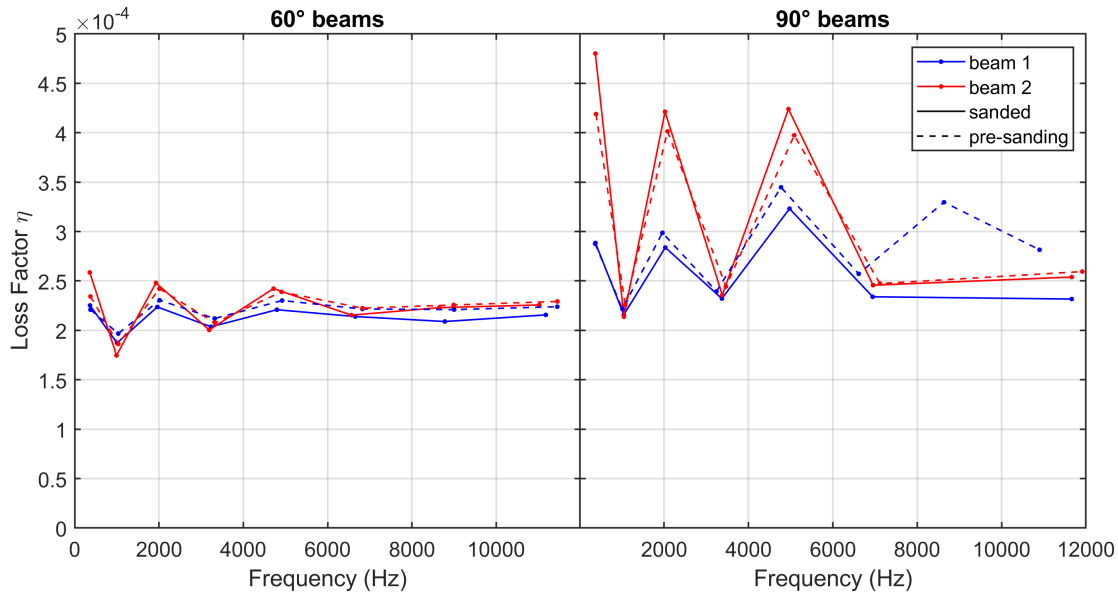
Figure 4: *Loss factor data for all four AM beams. The dotted lines show the loss factors for the corresponding beams before being sanded. Beams 1 and 2 correspond to those labeled "–1" and "–2" in Fig. 2.*
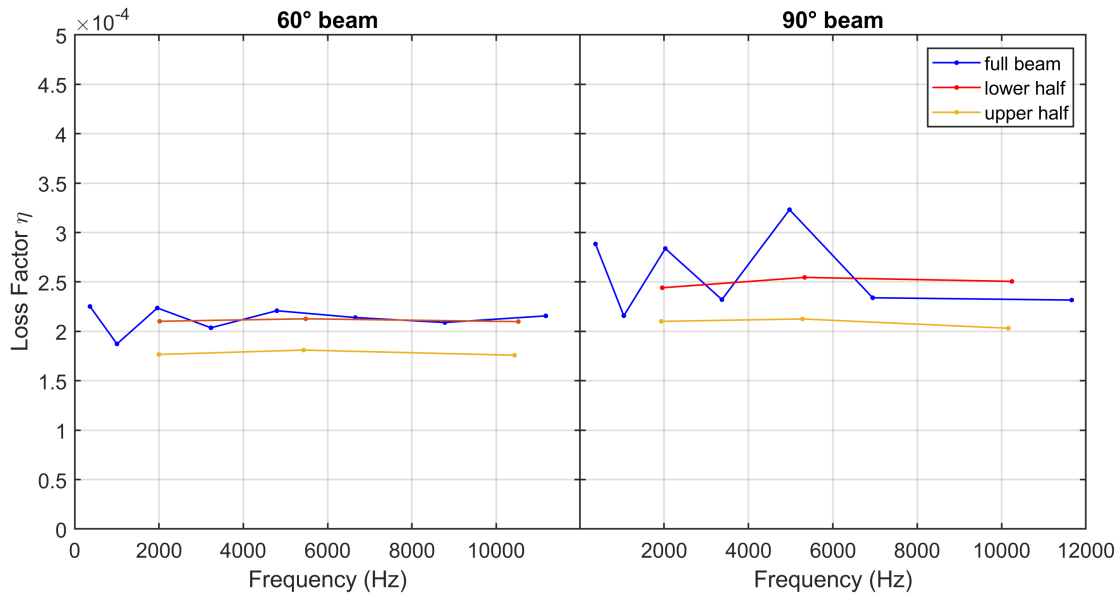
Figure 5: *Loss factor data for the 13 cm beams against their respective 30 cm counterpart.*

These measurements are compared to those made with traditionally formed steel and stainless steel beams in Fig. 6. We see that the 316L AM samples better reflect the flat nature of the 304 stainless steel beam while 1018 steel has a downward trend, a behavior more in line with Zener's model. Another 1018 steel beam, whose surface has been anodized with zinc, is also shown to provide another example of a physical property that can have a significant effect on the loss factor. Most interesting is how these results compare to Zener's model itself, shown in Fig. 7. The model is plotted using Eqs. (5) and (6), the material properties presented in Table 2, physical measurements for the dimensions of each beam, and 293 K as the ambient temperature. For each steel beam, our measurements are markedly higher than what Zener's model or the Lifshitz and Roukes model, given in Eqs. (7) and (8), predict.
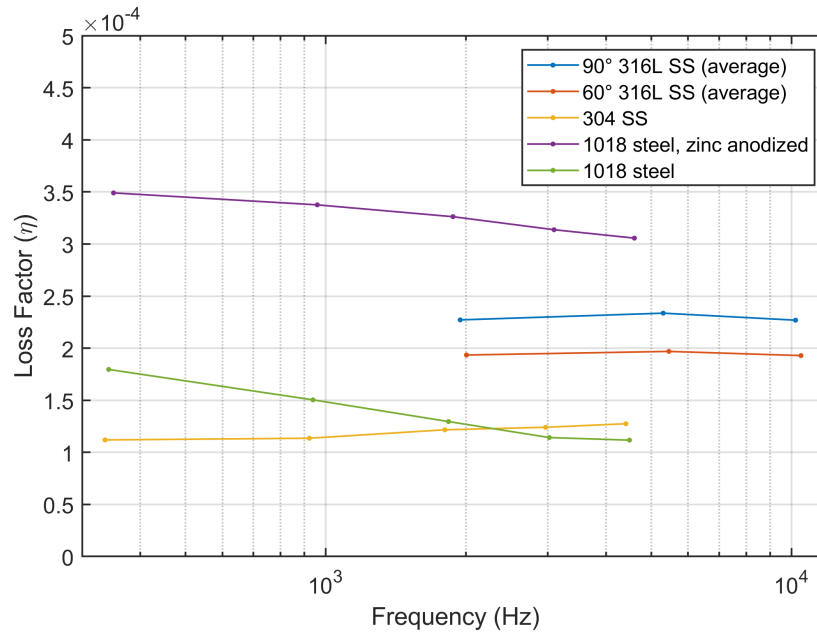
Figure 6: Loss factors for the 13 cm AM beams, averaged together, compared to measurements made with non-AM steel and stainless steel (SS) beams.
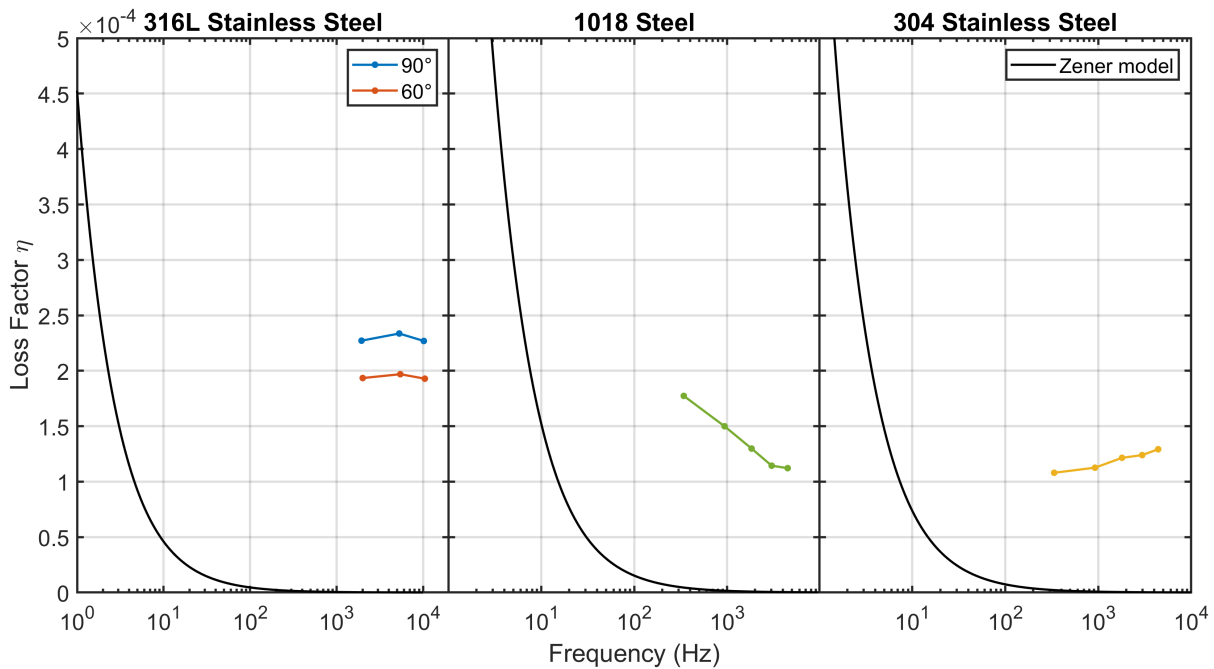

Figure 7: The 13 cm AM, steel, and stainless steel beams shown in Fig. 6 against Zener's model for their respective material properties.

5. CONCLUSIONS

Four Euler beams were constructed of 316L stainless steel using SLM, an AM technique, at two different build angles. Their internal damping was precisely measured for each resonant mode inside a vacuum chamber and compared to traditionally manufactured steel and stainless steel beams as well as to Zener's

Table 2: Steel material properties. The density is used to solve for the Young Modulus using Eq. (4) and the thermal constants are included to construct Zener's model given by Eqs. (5) and (6). Constants are approximate and aside from the density, weren't measured using our specific samples.

		1018 Steel	304 Stainless Steel	316L Stainless Steel
E	(GPa)	203	196	180
ρ	(kg m^{-3})	7830	7930	7730
α	(10^{-6} K^{-1})	12	17	16
C_s	(J kg^{-1} K^{-1})	450	500	500
κ	(W m^{-1} K^{-1})	50	16	15

model of thermoelasticity. The AM beams were also cut and remeasured in order to negotiate around a central discontinuity that arose in the SLM process, providing additional insight into how the material's damping differs before and after the interruption occurred.

Both the build angle and the interruption to the SLM procedure had a measurable effect on the internal damping of our 316L stainless steel beams, though we do not yet fully understand why these properties affect the internal damping in the way they do. It is also unclear why the steel beams, both manufactured traditionally and with AM, disagree with Zener's model. Perhaps thermoelastic currents are not the single dominant damping mechanism at these frequencies in steel as has been assumed. Alternatively, our approximation of an Euler beam at these dimensions may not work as well as it does for lighter materials such as aluminum. Further experimentation with thinner samples should help to validate or invalidate this model, though it should be noted that the resonant frequencies measured match those defined by Eq. 4. Nonetheless, these are encouraging preliminary results that promise great potential in studying the nuances of AM materials by measuring their internal damping.

ACKNOWLEDGMENTS

APPENDIX A

Figure 8 shows the loss factor measurements at the first five resonant frequencies of an aluminum Euler beam with string configurations corresponding to the first four structural beam modes. It can be seen that for the first mode (around 330 Hz), the first string configuration gives the lowest loss factor and therefore, the most accurate measurement for the internal damping. For the second mode, the second string configuration is best, and so on. A single string configuration cannot be used to study all the resonant modes since it does not match the nodal lines of each. This adds to the measured damping by dissipating energy. For resonant frequencies past the fourth mode, the minimum value between the four string configuration measurements is used.

Ideally, we would enforce simply-supported boundary conditions since all mode shapes of the beam would have nodes at the edges and multiple configurations wouldn't be needed. Unfortunately, we were unable to develop a setup which did this well and instead opted for the free-free approach with strings.

06 January 2025 19:24:35
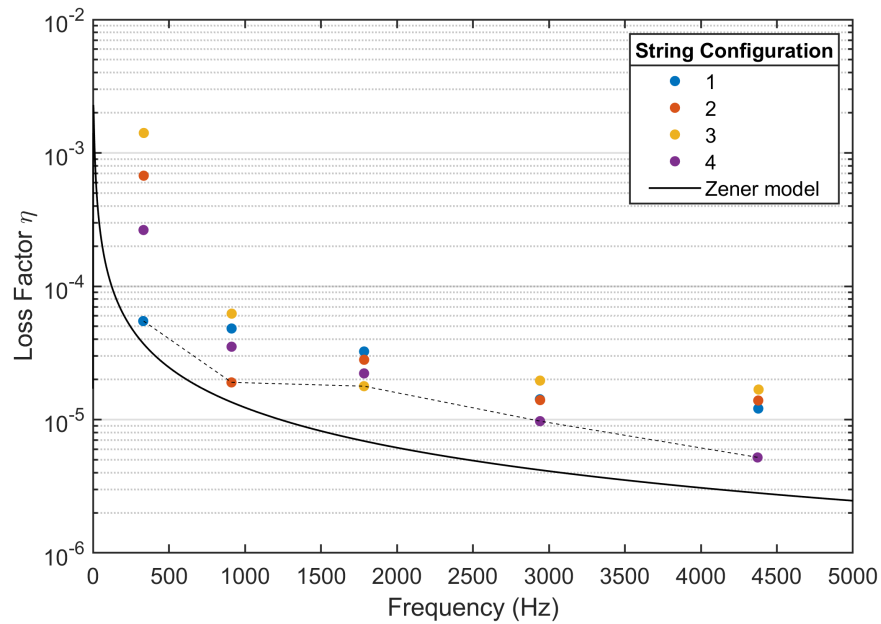
Figure 8: Loss factor measurements made with an aluminum Euler beam on each of the four string configurations. The best (minimum) measurements are connected by the dotted line and are compared to Zener's model of thermoelasticity in black.

REFERENCES

Casiano, M. J. (**2016**). "Extracting damping ratio from dynamic data and numerical solutions," Technical Report NASA/TM-2016-218227, https://ntrs.nasa.gov/citations/20170005173.

Lifshitz, R., and Roukes, M. L. (**2000**). "Thermoelastic damping in micro- and nanomechanical systems," Physical Review B **61**(8), 5600–5609, https://doi.org/10.1103/PhysRevB.61.5600.

Mills, J. T., Jensen, P. K., and Shepherd, M. R. (**2024**). "Effects of rarefied atmosphere on radiation damping in an aluminum euler beam," in *Proceedings of the 42nd IMAC*, Vol. 5.

Pierce, A. D. (**2010**). "Intrinsic damping, relaxation processes, and internal friction in vibrating systems," Proceedings of Meetings on Acoustics **9**(1), 065001, https://doi.org/10.1121/1.3449319.

Yang, L., Li, P., Fang, Y., and Ge, X. (**2021**). "A generalized methodology for thermoelastic damping in axisymmetric vibration of circular plate resonators covered by multiple partial coatings," Thin-Walled Structures **162**, 107576, https://doi.org/10.1016/j.tws.2021.107576.

Zacharias, C., Könke, C., and Guist, C. (**2022**). "A new efficient approach to simulate material damping in metals by modeling thermoelastic coupling," Materials **15**(5), 1706, https://doi.org/10.3390/ma15051706.

Zener, C. (**1937**). "Internal friction in solids, i. theory of internal friction in reeds," Phys. Rev. **52**(3), 230–235, https://doi.org/10.1103/PhysRev.52.230.

Zener, C. (**1938**). "Internal friction in solids, ii. general theory of thermoelastic internal friction," Phys. Rev. **53**(1), 90–99, https://doi.org/10.1103/PhysRev.53.90.